

# Dynamically Generated Synthetic Electric Fields for Photons

Petr Zapletal,<sup>1</sup> Stefan Walter,<sup>2,3</sup> and Florian Marquardt<sup>2,3</sup>

<sup>1</sup>*Cavendish Laboratory, University of Cambridge, Cambridge CB3 0HE, United Kingdom*

<sup>2</sup>*Max Planck Institute for the Science of Light, Staudtstraße 2, 91058 Erlangen, Germany*

<sup>3</sup>*Institute for Theoretical Physics, University Erlangen-Nürnberg, Staudtstraße 7, 91058 Erlangen, Germany*

Static synthetic magnetic fields give rise to phenomena including the Lorentz force and the quantum Hall effect even for neutral particles, and they have by now been implemented in a variety of physical systems. Moving towards fully dynamical synthetic gauge fields allows, in addition, for backaction of the particles' motion onto the field. If this results in a time-dependent vector potential, conventional electromagnetism predicts the generation of an electric field. Here, we show how synthetic electric fields for photons arise self-consistently due to the nonlinear dynamics in a driven system. Our analysis is based on optomechanical arrays, where dynamical gauge fields arise naturally from phonon-assisted photon tunneling. We study open, one-dimensional arrays, where synthetic magnetic fields are absent. However, we show that synthetic electric fields can be generated dynamically, which, importantly, suppress photon transport in the array. The generation of these fields depends on the direction of photon propagation, leading to a novel mechanism for a photon diode, inducing nonlinear nonreciprocal transport via dynamical synthetic gauge fields.

The field of cavity optomechanics, addressing the interaction between light and sound, has made rapid strides in recent years [1]. Experiments have shown ground state cooling [2, 3], measurements of motion with record sensitivity [4], efficient conversion between microwave and optical photons [5], dynamics of vibrations near exceptional points [6], and the control of single phonons [7], to name but a few achievements.

Due to the optomechanical interaction, mechanical vibrations can change the light frequency. During this process, the mechanical oscillation phase is imparted onto the light field. In this way, optomechanics can be used as a natural means to generate synthetic magnetic fields for photons, as was first suggested in Refs. [8, 9]. Together with reservoir engineering [10], these ideas form the theoretical basis underlying a recent series of pioneering experiments on optomechanical nonreciprocity [11–16]. While those still operate in few-mode setups, future extensions to optomechanical arrays (of the type proposed in [17–20]) will enable studies of photon transport on a lattice in the presence of an arbitrary tunable synthetic magnetic field [9]. A similar optomechanical design underlies the first proposal for engineered topological phonon transport in any platform [21]. All of these developments tie into the much wider field of synthetic magnetic fields and topologically protected nonreciprocal transport, first envisaged and implemented for cold atoms [22–25] and then for photons [26–32], phonons [21, 33–37], and other platforms [38, 39].

In these works, the gauge fields are fixed by external parameters, e.g., the phases of external driving beams. It was understood only recently that optomechanics provides a very natural platform for creating *dynamical* classical gauge fields [40]: if the mechanical resonator is not driven externally but rather undergoes limit-cycle oscillations, then the phase of those oscillations becomes a dynamical gauge field. This field is a new degree of freedom that can be influenced by the photons instead of being fixed externally. The possibility to engineer artificial

dynamical gauge fields has recently attracted attention also in different experimental platforms, such as ultracold atoms in optical lattices [41, 42], superconducting circuits [43, 44], cavity quantum electrodynamics [45], and trapped ions [46, 47].

If the dynamics results in a time-dependent vector potential, conventional electromagnetism dictates that this describes an electric field. In the present work, we show how a rather elementary optomechanical system offers the possibility of observing a synthetic electric field. This field is dynamically generated by the nonlinear coupled dynamics of the photons and the vibrational gauge field. It can arise even in a linear arrangement of coupled photon modes, a situation where a static vector potential does not have any effect, since it can be gauged away. Moreover, the appearance of the field turns out to depend on the direction of photon propagation. In this way, a novel mechanism for nonlinear nonreciprocal transport of photons (a photon diode) is uncovered. This works especially well in arrays, giving rise to a significant suppression of transport in the blockaded direction.

*Dynamical gauge fields for photons.* — The optomechanical interaction can be used to realize phonon-assisted photon tunneling, which, as we have shown previously, offers a natural route towards classical dynamical gauge fields for photons [40]. Photons hopping between optical modes  $\hat{a}_1$  and  $\hat{a}_2$  absorb or emit a phonon from a mechanical mode  $\hat{b}$ . A pictorial representation of this process is shown in Fig. 1a. Many implementations are conceivable (including photonic crystal devices, coupled toroids, and microwave circuits [1]), but a suitable realization might simply consist of the well-known membrane-in-the-middle setup [48, 49]. The basic phonon-assisted photon tunneling process is described by the Hamiltonian

$$\hat{H} = \sum_{j=1}^2 \nu_j \hat{a}_j^\dagger \hat{a}_j + \Omega \hat{b}^\dagger \hat{b} + J \left( \hat{b} \hat{a}_2^\dagger \hat{a}_1 + \text{h.c.} \right), \quad (1)$$

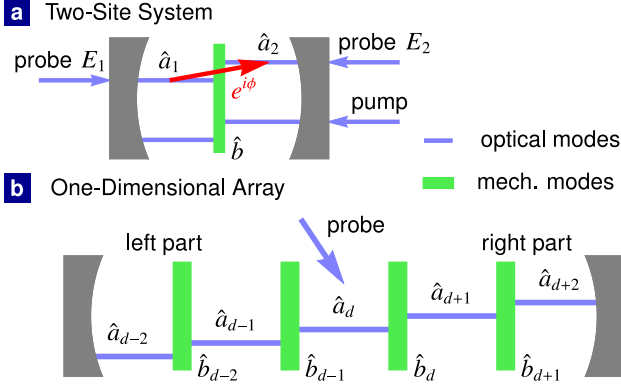


FIG. 1. (color) An optomechanical setup able to exhibit dynamically generated synthetic electric fields for photons. (a) A cavity with a movable membrane (green rectangle) in the middle. The mechanical mode  $\hat{b}$  undergoes self-oscillations (e.g. by pumping another optical mode on its blue sideband). Photons tunneling from the optical mode  $\hat{a}_1$  to  $\hat{a}_2$  (red arrow) absorb a phonon from the mechanical oscillation, thereby acquiring a phase shift set by the oscillation phase  $\phi$ . Photon transport through the setup can be probed by a laser injected into the modes  $\hat{a}_1$  or  $\hat{a}_2$ . The optical modes' frequencies are represented by the blue lines. (b) A one-dimensional array, with optical modes  $\hat{a}_j$  of increasing frequency. Mechanical modes  $\hat{b}_j$  assist tunneling between modes  $\hat{a}_j$  and  $\hat{a}_{j+1}$ . Some mode in the middle,  $\hat{a}_d$ , is driven by a laser (blue arrow), probing photon transport both towards the left and right.

where  $\nu_j$  are the optical frequencies of modes  $\hat{a}_j$ ,  $\Omega$  is the frequency of the mechanical oscillator and  $J$  is the tunneling amplitude. In the following, we set  $\hbar = 1$  (later reinstated during our discussion of experimentally realistic values). The optical frequencies are detuned from one another to suppress direct tunneling between the optical modes. To select the phonon-assisted photon tunneling, the mechanical frequency is tuned to match the optical frequency difference  $\Omega \approx |\nu_2 - \nu_1|$ . The Hamiltonian (1) is valid within the rotating-wave approximation for  $\nu_2 > \nu_1$  and  $\Omega \gg \kappa, J, JB$ , where  $\kappa$  is the photon decay rate and  $B$  is the amplitude of the mechanical oscillations  $B = |\langle \hat{b} \rangle|$ .

Optomechanical generation of *static* gauge fields was first discussed in Ref. [9]. The ‘‘wavelength conversion’’ scheme analyzed there features the Hamiltonian (1), and it can be readily implemented in optomechanical crystals [50, 51] or the membrane-cavity setup [48, 49].

To implement *dynamical* gauge fields for photons, the mechanical mode has to perform limit-cycle oscillations with a large fixed amplitude  $B$  and a free phase  $\phi$  [40], such that  $\langle \hat{b} \rangle = B e^{i\phi}$ . The limit-cycle oscillations can be generated by pumping an ancillary optical mode, situated at a different frequency, on the blue sideband [52] (see Fig. 1a). In a limit cycle, the mechanical oscillation phase is able to evolve according to its own dynamics. Thus the phase turns into a dynamical gauge field, being influenced by the photon transport and acting back on the photons. This system, composed of two opti-

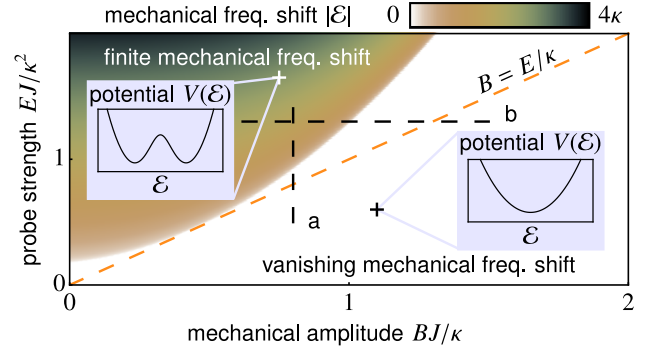


FIG. 2. Phase diagram for dynamically generated synthetic electric fields in a two-site system. In the white region, the electric field  $\mathcal{E}$  vanishes in the steady state. If mode  $\hat{a}_1$  with the lower optical frequency is driven, the field  $\mathcal{E}$  bifurcates in the colored region to finite stationary values. Their absolute values are indicated by the color scale. The blue insets show the shape of the effective potential  $V(\mathcal{E})$  that determines the steady-state value of  $\mathcal{E}$ . The dashed black lines denote the cuts along which the field and the optical amplitudes are plotted in Fig. 3. The dashed orange line indicates a lower bound for the laser amplitude required to observe nonzero fields.

cal modes and one mechanical mode, can be used as a building block for optomechanical arrays with dynamical gauge fields for photons [40]. In the membrane setup of Fig. 1a, particularly efficient doubly-resonant pumping of limit cycles is possible (see also Ref. [53]).

*Dynamics and synthetic electric fields.* — Let us start by analyzing the dynamics of the gauge field in a two-site system described by the Hamiltonian (1), with the mechanical oscillator performing limit-cycle oscillations. The optical mode  $\hat{a}_j$  can be driven by a laser of amplitude  $E_j$  at frequency  $\nu_{D,j}$ , to probe photon transport through the system. The optical fields and the mechanical amplitude will be assumed large enough such that quantum noise effects can be neglected, which is an excellent approximation for all the existing optomechanical experiments studying nonlinear dynamics.

Following Ref. [40], the coupled classical equations of motion for the optical amplitudes  $a_j = \langle \hat{a}_j \rangle$  and the mechanical phase  $\phi$  read

$$\dot{\phi} = \Delta_M - \frac{J}{B} \text{Re} [a_1^* a_2 e^{-i\phi}], \quad (2)$$

$$\dot{a}_1 = i\Delta_1 a_1 - iE_1 - iJB e^{-i\phi} a_2 - \frac{\kappa}{2} a_1, \quad (3)$$

$$\dot{a}_2 = i\Delta_2 a_2 - iE_2 - iJB e^{i\phi} a_1 - \frac{\kappa}{2} a_2, \quad (4)$$

where  $\Delta_j = \nu_{D,j} - \nu_j$  and  $\Delta_M = \nu_{D,2} - \nu_{D,1} - \Omega$  are optical and mechanical detunings, respectively (switching to suitable rotating frames). Here the mechanical mode is in the frame rotating with the frequency  $\nu_{D,2} - \nu_{D,1}$ . The limit-cycle amplitude  $B$  of the mechanical oscillator is considered fixed, determined by the optical pump. These equations form the starting point of our analysis.

To build physical intuition, let us first consider the

case where both optical modes are driven. Then, the resulting beat note gives rise to an oscillating force  $F \propto J|a_1||a_2| \cos((\nu_{D,2} - \nu_{D,1})t + \theta_{1,2})$  acting on the mechanical oscillator, as can be deduced directly from the Hamiltonian (1). Here  $\theta_{1,2} = \theta_2 - \theta_1$  is the difference of the phases  $\theta_j$  of the modes  $a_j$ . While the effect of this on the large mechanical amplitude  $B$  is negligible, the mechanical phase feels a drift term  $\dot{\phi} = -\frac{J}{B}|a_1||a_2| \cos(\phi - \theta_{1,2})$ , according to Eq. (2). As a result, one observes phase-locking [18]: the mechanical phase  $\phi$  tries to be close to the optical phase difference  $\theta_{1,2}$ , provided the detuning  $\Delta_M$  between the mechanical frequency and the optical frequency difference is sufficiently small.

By contrast, if only one mode is laser-driven, no external phase is imprinted. The mechanical oscillator is free to pick any phase despite the interaction with the optical modes. The phase now forms a classical gauge field with  $U(1)$  symmetry. The gauge transformation

$$\phi \mapsto \phi + \chi_2 - \chi_1, \quad (5)$$

$$a_j \mapsto a_j e^{i\chi_j}, \quad \text{for } j = 1, 2, \quad (6)$$

generates a new valid solution of the dynamical equations, for any real function  $\chi_j(t)$ . The transformation also preserves the optical and mechanical frequencies whenever is time-independent, i.e.,  $\chi_j = \text{const}$ . On the other hand, if the  $\chi_j$  are time-dependent, Eqs. (5) and (6) have to be supplemented by a shift in the frequencies:  $\Omega \mapsto \Omega + \dot{\chi}_1 - \dot{\chi}_2$  and  $\nu_j \mapsto \nu_j - \dot{\chi}_j$ . We note the relation to conventional electromagnetism, where an electric field can be represented either as a time-dependent vector potential or a scalar potential gradient. As a consequence, any time evolution of the mechanical phase  $\phi$  can be viewed as generating a synthetic electric field

$$\mathcal{E} = \dot{\phi} \quad (7)$$

for photons. For example, if mode 1 is laser-driven, we can set  $\chi_1 = 0$ ,  $\chi_2 = -\phi$ , which will result in a description where the mechanical phase is now static, but  $\nu_2 \mapsto \nu_2 + \mathcal{E}$ . Thus, physically, this synthetic electric field  $\mathcal{E}$  describes an effective optical frequency shift generated by an evolving mechanical phase. As we will show, this has important consequences for the photon transport.

*Dynamical phase diagram.* — In the situation studied here,  $\mathcal{E}$  is not prescribed externally but is the result of a dynamical process resulting from the coupling of the optical and mechanical modes. The optical modes induce the force  $F$  acting on the mechanical phase. The resulting phase evolution may cause a synthetic field  $\mathcal{E}$  which effectively modifies the optical frequency difference and, consequently, the population of the optical modes.

The results of the dynamical analysis are shown in Fig. 2. We depict the steady state value of the synthetic field  $\mathcal{E}$ , which can be zero or finite, delineating two qualitatively different types of behavior.

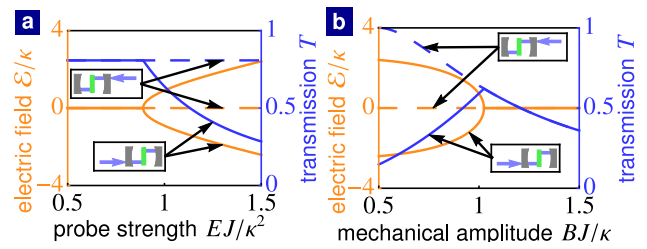


FIG. 3. Cuts in the parameter space denoted by the dashed black lines in Fig. 2. The mechanical frequency shift  $\mathcal{E}$  (orange line) and the optical transmission  $T$  (blue line). Mode  $a_1$  with the lower optical frequency is driven (solid line) or mode  $a_2$  with the higher optical frequency is driven (dashed line).

To understand this diagram, we first note that the equations of motion are not symmetric under exchange of the optical modes: it matters which direction a photon has to travel to absorb a phonon. As a consequence, different asymptotic behaviors are reached depending on which mode is driven by the laser (of amplitude  $E$ ). In Fig. 2, we assumed the lower-frequency mode to be driven. Moreover, we consider the fully resonant situation where the physical effects are most pronounced, as both the optical driving and the phonon-assisted photon tunneling process are resonant ( $\Delta_M = \Delta_1 = \Delta_2 = 0$ , in the rotating frame  $\nu_{D,j} = \nu_j$  for the mode  $j$  that is not driven by any laser). For this setting, the system always converges to a steady state for any values of the system parameters  $B$ ,  $J$ ,  $E$ , and  $\kappa$  and either mode being driven. The steady-state value of  $\mathcal{E}$  turns out to depend only on two dimensionless parameters: the rescaled limit-cycle amplitude  $BJ/\kappa$  and the rescaled laser amplitude  $EJ/\kappa^2$ .

The analysis of the nonlinear dynamics can be made more intuitive by “integrating out” the optical modes. This leaves us with an effective potential  $V(\mathcal{E})$ , whose minima determine the possible steady-state values of the field  $\mathcal{E}$  (see the supplementary material [54] for the full analytical expression):

$$\dot{\mathcal{E}} = -\frac{dV(\mathcal{E})}{d\mathcal{E}} = 0. \quad (8)$$

In the white region of the phase diagram, Fig. 2, the potential  $V(\mathcal{E})$  has a single minimum at  $\mathcal{E} = 0$  (see the blue inset). There, the field  $\mathcal{E}$  vanishes in the steady state: the gauge field is stationary and can be gauged away by a time-independent gauge transformation. This state becomes unstable in the colored region of the phase diagram, where the potential  $V(\mathcal{E})$  has two minima at finite values of  $\mathcal{E}$ . The field  $\mathcal{E}$  can develop such a nonzero value only for  $BJ/\kappa < EJ/\kappa^2$ , i.e.,  $B < E/\kappa$  (above the dashed orange line). In terms of physical parameters, this means that the photon occupation of the driven optical mode has to exceed the phonon number in the limit-cycle oscillation.

By contrast, if the mode with the higher optical fre-

quency,  $a_2$ , is driven, the potential  $V(\mathcal{E})$  *always* has a single minimum at  $\mathcal{E} = 0$  for any values of the system parameters. The (static) gauge field can always be gauged away. This situation corresponds to a direct photon tunneling between the two optical modes, with an effective tunneling amplitude  $JB$ .

Linear stability analysis and numerical simulations of the equations of motion were used to confirm convergence to these steady states. The states are not qualitatively changed for finite mechanical and laser detunings (see the supplementary material [54]).

We now study the effects of the dynamically generated synthetic field on the light transport. To this end, we define the transmission  $T$  as the ratio of the output power leaking from the non-driven mode, which is equal to  $\kappa|a_2|^2$  (if mode 1 is driven) or  $\kappa|a_1|^2$  (if mode 2 is driven), and the driving power equal to  $E^2/\kappa$ . We find that

$$T = \frac{\frac{B^2 J^2}{\kappa^2}}{\left(\frac{B^2 J^2}{\kappa^2} + \frac{1}{4}\right)^2 + \frac{1}{4\kappa^2} \mathcal{E}^2}, \quad (9)$$

which is suppressed when a finite field  $\mathcal{E}$  detunes the tunneling process from resonance. In Figs. 3a, 3b, the transmission  $T$  (blue line) and the synthetic field  $\mathcal{E}$  (orange line) are depicted along cuts in the phase diagram (denoted by the dashed black lines in Fig. 2).

We have demonstrated for the two-site system that when light propagates to higher optical frequencies the phonon-assisted photon tunneling is suppressed due to the synthetic electric field. On the other hand, we find that the field always vanishes when light propagates towards lower optical frequencies. In this way, dynamical gauge fields give rise to a new mechanism for realizing a “photon diode” where the nonlinear light transport is nonreciprocal.

In the following, we show that this effect can also be used to control light propagation in a one-dimensional array.

*Nonlinear nonreciprocal light transport in a one-dimensional array.* — We now consider an array, depicted in Fig. 1b in terms of a realization using a stack of membranes inside a cavity. The sites of the array support optical modes  $a_j$  whose frequencies  $\nu_j$  increase with the site index  $j = 1, \dots, n$  (the spacing between membranes becomes progressively smaller). We assume that the phonon-assisted photon tunneling processes are resonant:  $\Omega_j = \nu_{j+1} - \nu_j$ , where  $\Omega_j$  is the frequency of the mechanical oscillator assisting tunneling between modes  $\hat{a}_j$  and  $\hat{a}_{j+1}$ . Specifically, we will consider a situation where some interior optical mode  $j = d$  is driven resonantly from the side, to study the light propagation towards the left ( $j < d$ ), and towards the right ( $j > d$ ). Alternatively to membrane stacks, suitably designed coupled cavity arrays in optomechanical crystals could naturally implement such a setup.

We study the dynamics of the one-dimensional array by numerically solving the classical equations of motion

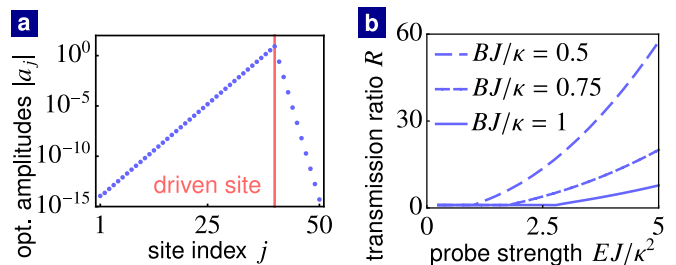


FIG. 4. Light transport in a 1D array with a dynamical gauge field – generation of a barrier for photon transport induced by a synthetic electric field. (a) The absolute values of the optical amplitudes  $|a_j|$  as a function of position for  $EJ/\kappa^2 = 10$ , and  $BJ/\kappa = 1$ . Note: the graph is plotted on logarithmic scale. The solid red line denotes the driven site (The graph is plotted for  $n = 50$  sites, site  $d = 40$  being driven). (b) Ratio  $R = |a_{d-1}/a_{d+1}|^2$  of the optical amplitudes to the left and to the right from driven site  $j = d$ . At  $m$  sites distance from the driven site, the ratio is exponentially increased, to  $R^m$ . (The graph is plotted for  $n = 79$  sites, site  $d = 40$  being driven).

for the optical amplitudes  $a_j = \langle \hat{a}_j \rangle$  and the mechanical phases  $\phi_j$ . The mechanical oscillators are again assumed to perform limit cycle oscillations  $\langle \hat{b}_j \rangle = B e^{i\phi_j}$  with free phases and with a constant amplitude  $B$  equal for all mechanical oscillators (the full equations of motion are a straightforward extension of Eqs. (2), (3), and (4); see the supplementary material [54]). The system converges to a steady state for any values of the parameters  $EJ/\kappa^2$  and  $BJ/\kappa$ .

Fig. 4a shows the result of the simulations: for sufficiently large laser drive, the system switches into a state where a synthetic field  $\mathcal{E}$  develops in the right part of the array. This is the direction where photons need to gain energy when tunneling, and where we already saw in the two-site system that (i) a finite field can develop, and (ii) it can detune and suppress photon transport. In the array, this results in a rapid exponential suppression of light intensity. By contrast, light easily propagates towards the left, where  $\mathcal{E}$  remains zero.

This results in a suppression of light propagation depending on the direction. To quantify this effect, we plot in Fig. 4b  $R = |a_{d-1}/a_{d+1}|^2$  corresponding to the ratio of transmission to the sites adjacent to the driven site  $j = d$  as a function of the laser amplitude  $EJ/\kappa^2$  for different limit-cycle amplitudes  $BJ/\kappa$ . The isolation ratio increases exponentially with a distance from the driven site (see Fig. 4a). At  $m$  sites distance from the driven site, the ratio is exponentially increased, to  $R^m$ . The suppression of light propagation to the right, i.e.,  $R > 1$ , is achieved only above a certain threshold value of the laser amplitude. Below this threshold,  $R$  is equal to unity, and light propagates symmetrically in both directions. The threshold value depends on the value of the limit-cycle amplitude. Above the threshold, larger suppression can be achieved by increasing the laser amplitude.

The presented analysis shows that the asymmetry of

the phonon-assisted photon tunneling can be used to implement light propagation with a preferred direction.

*Experimental parameters required for generating the synthetic electric field.* — We now estimate that the synthetic electric field can be observed for experimentally realistic parameters. For the membrane-in-the-middle setup, feasible experimental parameters are  $\kappa \approx 300$  kHz,  $J \approx 1$  Hz, a zero-point fluctuation amplitude of  $x_{\text{ZPF}} \approx 10^{-15}$  m and a number of photons in the cavity of order  $(E/\kappa)^2 \sim 10^{10}$  [49]. A typical number of phonons in a mechanical mode performing self-oscillations driven well above the threshold is  $B^2 \sim (\kappa/J)^2 \sim 10^{10}$  and a corresponding real oscillation amplitude is  $2x_{\text{ZPF}}B \sim 100$  pm [52]. The two optical modes considered in our model can be represented by hybridized transverse modes of the cavity with an avoided crossing [49]. The splitting of their frequencies  $\approx 200$  kHz can match the frequency of the mechanical mode. For these experimental parameters, the laser amplitude  $EJ/\kappa^2 \sim 1$  and the limit-cycle amplitude  $BJ/\kappa \sim 1$  are promising for observing the finite synthetic electric field (see the phase diagram in Fig. 2). The number of phonons can be decreased below the number of

photons in the driven optical mode by driving the mechanical self-oscillations closer to threshold [52], fulfilling the necessary condition for obtaining a finite synthetic electric field (Fig. 2).

*Conclusions.* — While synthetic gauge fields for photons have been investigated thoroughly in recent years, little has been known about the dynamical situation. In this work, we have uncovered how a synthetic electric field can be spontaneously created, in a readily realizable optomechanical setup. The resulting nonlinear photon-diode type of nonreciprocal transport can lead to a large isolation ratio, especially in arrays. Our numerical simulations indicate that similar effects can also be observed in two-dimensional square arrays. In the future, one might study how these phenomena can affect the synchronization dynamics in lattices of coupled optomechanical limit-cycle oscillators [18, 55, 56].

We thank A. Nunnenkamp and J. Harris for useful comments, and O. Hart for a careful reading of the manuscript. This work was supported by the European Union's Horizon 2020 research and innovation programme under grant agreement No 732894 (FET Proactive HOT).

- 
- [1] M. Aspelmeyer, T. J. Kippenberg, and F. Marquardt, *Rev. Mod. Phys.* **86**, 1391 (2014).
- [2] J. Chan, T. P. M. Alegre, A. H. Safavi-Naeini, J. T. Hill, A. Krause, S. Gröblacher, M. Aspelmeyer, and O. Painter, *Nature* **478**, 89 (2011).
- [3] J. D. Teufel, T. Donner, D. Li, J. W. Harlow, M. S. Allman, K. Cicak, A. J. Sirois, J. D. Whittaker, K. W. Lehnert, and R. W. Simmonds, *Nature* **475**, 359 (2011).
- [4] D. J. Wilson, V. Sudhir, N. Piro, R. Schilling, A. Ghadimi, and T. J. Kippenberg, *Nature* **524**, 325 (2015).
- [5] R. W. Andrews, R. W. Peterson, T. P. Purdy, K. Cicak, R. W. Simmonds, C. A. Regal, and K. W. Lehnert, *Nat. Phys.* **10**, 321 (2014).
- [6] H. Xu, D. Mason, L. Jiang, and J. G. E. Harris, *Nature* **537**, 80 (2016).
- [7] S. Hong, R. Riedinger, I. Marinković, A. Wallucks, S. G. Hofer, R. A. Norte, M. Aspelmeyer, and S. Gröblacher, *Science* **358**, 203 (2017).
- [8] M. Hafezi and P. Rabl, *Opt. Express* **20**, 7672 (2012).
- [9] M. Schmidt, S. Kessler, V. Peano, O. Painter, and F. Marquardt, *Optica* **2**, 635 (2015).
- [10] A. Metelmann and A. A. Clerk, *Phys. Rev. X* **5**, 021025 (2015).
- [11] J. Kim, M. C. Kuzyk, K. Han, H. Wang, and G. Bahl, *Nat. Phys.* **11**, 275 (2015).
- [12] Z. Wang, L. Shi, Y. Liu, X. Xu, and X. Zhang, *Sci. Rep.* **5**, 8657 (2015).
- [13] F. Ruesink, M.-A. Miri, A. Alù, and E. Verhagen, *Nat. Commun.* **7**, 13662 (2016).
- [14] K. Fang, J. Luo, A. Metelmann, M. H. Matheny, F. Marquardt, A. A. Clerk, and O. Painter, *Nat. Phys.* **13**, 465 (2017).
- [15] N. R. Bernier, L. D. Tóth, A. Koottandavida, M. A. Ioannou, D. Malz, A. Nunnenkamp, A. K. Feofanov, and T. J. Kippenberg, *Nat. Commun.* **8**, 604 (2017).
- [16] S. Barzanjeh, M. Wulf, M. Peruzzo, M. Kalaei, P. B. Dieterle, O. Painter, and J. M. Fink, *Nat. Commun.* **8**, 953 (2017).
- [17] D. E. Chang, A. H. Safavi-Naeini, M. Hafezi, and O. Painter, *New J. Phys.* **13**, 023003 (2011).
- [18] G. Heinrich, M. Ludwig, J. Qian, B. Kubala, and F. Marquardt, *Phys. Rev. Lett.* **107**, 043603 (2011).
- [19] A. Xuereb, C. Genes, and A. Dantan, *Phys. Rev. Lett.* **109**, 223601 (2012).
- [20] M. Ludwig and F. Marquardt, *Phys. Rev. Lett.* **111**, 073603 (2013).
- [21] V. Peano, C. Brendel, M. Schmidt, and F. Marquardt, *Phys. Rev. X* **5**, 031011 (2015).
- [22] D. Jaksch and P. Zoller, *New J. Phys.* **5**, 56 (2003).
- [23] Y.-J. Lin, R. L. Compton, K. Jiménez-García, J. V. Porto, and I. B. Spielman, *Nature* **462**, 628 (2009).
- [24] M. Aidelsburger, M. Atala, S. Nascimbène, S. Trotzky, Y.-A. Chen, and I. Bloch, *Phys. Rev. Lett.* **107**, 255301 (2011).
- [25] M. Aidelsburger, M. Atala, M. Lohse, J. T. Barreiro, B. Paredes, and I. Bloch, *Phys. Rev. Lett.* **111**, 185301 (2013).
- [26] F. D. M. Haldane and S. Raghu, *Phys. Rev. Lett.* **100**, 013904 (2008).
- [27] Z. Wang, Y. Chong, J. D. Joannopoulos, and M. Soljačić, *Nature* **461**, 772 (2009).
- [28] M. Hafezi, E. A. Demler, M. D. Lukin, and J. M. Taylor, *Nat. Phys.* **7**, 907 (2011).
- [29] K. Fang, Z. Yu, and S. Fan, *Nat. Photonics* **6**, 782 (2012).
- [30] M. C. Rechtsman, J. M. Zeuner, A. Tünnermann, S. Nolte, M. Segev, and A. Szameit, *Nat. Photonics* **7**, 153 (2013).

- [31] M. Hafezi, S. Mittal, J. Fan, A. Migdall, and J. M. Taylor, *Nat. Photonics* **7**, 1001 (2013).
- [32] S. Mittal, J. Fan, S. Faez, A. Migdall, J. M. Taylor, and M. Hafezi, *Phys. Rev. Lett.* **113**, 087403 (2014).
- [33] L. M. Nash, D. Kleckner, A. Read, V. Vitelli, A. M. Turner, and W. T. M. Irvine, *Proc. Natl. Acad. Sci. U.S.A.* **112**, 14495 (2015).
- [34] R. Süssstrunk and S. D. Huber, *Science* **349**, 47 (2015).
- [35] P. Wang, L. Lu, and K. Bertoldi, *Phys. Rev. Lett.* **115**, 104302 (2015).
- [36] C. Brendel, V. Peano, O. J. Painter, and F. Marquardt, *Proc. Natl. Acad. Sci. U.S.A.* **114**, E3390 (2017).
- [37] C. Brendel, V. Peano, O. Painter, and F. Marquardt, *Phys. Rev. B* **97**, 020102 (2018).
- [38] N. Goldman, G. Juzeliūnas, P. Öhberg, and I. B. Spielman, *Rep. Prog. Phys.* **77**, 126401 (2014).
- [39] M. J. Hartmann, *J. Opt.* **18**, 104005 (2016).
- [40] S. Walter and F. Marquardt, *New J. Phys.* **18**, 113029 (2016).
- [41] D. Banerjee, M. Dalmonte, M. Müller, E. Rico, P. Stebler, U.-J. Wiese, and P. Zoller, *Phys. Rev. Lett.* **109**, 175302 (2012).
- [42] E. Zohar, J. I. Cirac, and B. Reznik, *Rep. Prog. Phys.* **79**, 014401 (2016).
- [43] D. Marcos, P. Rabl, E. Rico, and P. Zoller, *Phys. Rev. Lett.* **111**, 110504 (2013).
- [44] D. Marcos, P. Widmer, E. Rico, M. Hafezi, P. Rabl, U. J. Wiese, and P. Zoller, *Annals of Physics* **351**, 634 (2014).
- [45] K. E. Ballantine, B. L. Lev, and J. Keeling, *Phys. Rev. Lett.* **118**, 045302 (2017).
- [46] P. Hauke, D. Marcos, M. Dalmonte, and P. Zoller, *Phys. Rev. X* **3**, 041018 (2013).
- [47] E. A. Martinez, C. A. Muschik, P. Schindler, D. Nigg, A. Erhard, M. Heyl, P. Hauke, M. Dalmonte, T. Monz, P. Zoller, and R. Blatt, *Nature* **534**, 516 (2016).
- [48] J. D. Thompson, B. M. Zwickl, A. M. Jayich, F. Marquardt, S. M. Girvin, and J. G. E. Harris, *Nature* **452**, 72 (2008).
- [49] J. C. Sankey, C. Yang, B. M. Zwickl, A. M. Jayich, and J. G. E. Harris, *Nat. Phys.* **6**, 707 (2010).
- [50] A. H. Safavi-Naeini and O. Painter, *New J. Phys.* **13**, 013017 (2011).
- [51] T. K. Paraíso, M. Kalaei, L. Zang, H. Pfeifer, F. Marquardt, and O. Painter, *Phys. Rev. X* **5**, 041024 (2015).
- [52] F. Marquardt, J. G. E. Harris, and S. M. Girvin, *Phys. Rev. Lett.* **96**, 103901 (2006).
- [53] H. Wu, G. Heinrich, and F. Marquardt, *New J. Phys.* **15**, 123022 (2013).
- [54] See supplementary material for the derivation of the effective potential for the sythetic electric field and the equations of motion for the one-dimensional array..
- [55] R. Lauter, C. Brendel, S. J. M. Habraken, and F. Marquardt, *Phys. Rev. E* **92**, 012902 (2015).
- [56] T. Weiss, S. Walter, and F. Marquardt, *Phys. Rev. A* **95**, 041802 (2017).

# Dynamically generated Synthetic Electric Fields for Photons – Supplementary material

## STEADY STATES OF THE TWO-SITE SYSTEM

In this section, we analyze the steady states of the two-site system. They are stationary solutions of the equations of motion (Eq. (2), Eq. (3), and Eq. (4) in the main text) constant in time. We first apply a time-dependent gauge transformation to remove the time-evolution of the mechanical phase. Then we find a stationary condition for the synthetic electric field  $\mathcal{E}$ . Finally, we use an effective potential for the synthetic electric field to study the stability of its stationary solutions.

As mentioned in the main text, we assume that only one mode is driven. We label the driven mode by the index  $k = 1, 2$ . Driving strengths can then be expressed as  $E_j = E \delta_{j,k}$  for  $j = 1, 2$ , where  $\delta_{j,k}$  is the Kronecker delta. The detuning of the non-driven mode can be set to zero, since there is no driving frequency. Therefore, the optical detunings can be expressed as  $\Delta_j = \Delta_O \delta_{j,k}$ . The time evolution of the mechanical phase can be completely removed by the time-dependent gauge transformation

$$\phi = \tilde{\phi} + \chi, \quad (\text{S1})$$

$$a_1 = \tilde{a}_1 e^{-i\chi \delta_{2,k}}, \quad (\text{S2})$$

$$a_2 = \tilde{a}_2 e^{i\chi \delta_{1,k}}, \quad (\text{S3})$$

where  $\chi$  is the time dependent gauge parameter,  $\tilde{\phi} = \text{const}$ . The time-dependent gauge transformation leaves the absolute values of the optical amplitudes unchanged. The time evolution of  $\phi$  causes a mechanical frequency shift  $\dot{\chi} = \dot{\phi}$  representing the synthetic electric field  $\mathcal{E} = \dot{\chi}$ . Since the frequency of the non-driven optical mode is generated as a side band to the driving frequency, it is shifted by  $(\delta_{2,k} - \delta_{1,k}) \mathcal{E}$ . The mechanical frequency shift  $\mathcal{E}$  represents a synthetic electric field for photons. Note that the driven mode,  $a_k$ , is forced to oscillate with the frequency of the laser drive, and thus it does not experience any frequency shift.

To provide the fixed point analysis for the both cases  $k = 1, 2$  at once, we use general indexes  $(k, l) \in \{(1, 2), (2, 1)\}$  to label the optical modes and we use the notation  $\tilde{\phi} = \tilde{\phi}_{1,2} = -\tilde{\phi}_{2,1}$ . According to the gauge transformation (S1), (S2), and (S3), the equations of motion transform to

$$\dot{\tilde{\phi}}_{k,l} = (\delta_{2,k} - \delta_{1,k}) \left( \mathcal{E} - \Delta_M + \frac{J}{B} \text{Re} \left[ \tilde{a}_k^* \tilde{a}_l e^{-i\tilde{\phi}_{k,l}} \right] \right), \quad (\text{S4})$$

$$\dot{\tilde{a}}_k = i\Delta_O \tilde{a}_k - iE - iJB e^{-i\tilde{\phi}_{k,l}} \tilde{a}_l - \frac{\kappa}{2} \tilde{a}_k, \quad (\text{S5})$$

$$\dot{\tilde{a}}_l = i(\delta_{2,k} - \delta_{1,k}) \mathcal{E} \tilde{a}_l - iJB e^{i\tilde{\phi}_{k,l}} \tilde{a}_k - \frac{\kappa}{2} \tilde{a}_l. \quad (\text{S6})$$

As a direct consequence of the gauge choice,  $\dot{\tilde{\phi}}_{k,l} = 0$ . Taking the time derivative of Eq. (S4), we obtain the equation of motion for the mechanical frequency shift

$$\dot{\mathcal{E}} = -\kappa (\mathcal{E} - \Delta_M) + \frac{EJ}{B} \text{Im} \left[ \tilde{a}_l e^{-i\tilde{\phi}_{k,l}} \right] + \frac{J}{B} ((\delta_{2,k} - \delta_{1,k}) \mathcal{E} - \Delta_O) \text{Im} \left[ \tilde{a}_k^* \tilde{a}_l e^{-i\tilde{\phi}_{k,l}} \right]. \quad (\text{S7})$$

To find stationary solutions of the equations of motion (S5), (S6), and (S7), we first use that the equations (S5) and (S6) are linear in terms of optical amplitudes. For a given mechanical frequency shift  $\mathcal{E}$ , the stationary optical amplitudes read

$$\tilde{a}_k = E \frac{(\delta_{2,k} - \delta_{1,k}) \mathcal{E} + i\frac{\kappa}{2}}{-J^2 B^2 + (\delta_{2,k} - \delta_{1,k}) \mathcal{E} \Delta_O - \left(\frac{\kappa}{2}\right)^2 + i\frac{\kappa}{2} [(\delta_{2,k} - \delta_{1,k}) \mathcal{E} + \Delta_O]}, \quad (\text{S8})$$

$$\tilde{a}_l = \frac{JB e^{i\tilde{\phi}_{k,l}}}{(\delta_{2,k} - \delta_{1,k}) \mathcal{E} + i\frac{\kappa}{2}} \tilde{a}_k. \quad (\text{S9})$$

Note that the ratio  $|a_l/a_k| = 2JB/\sqrt{4\mathcal{E}^2 + \kappa^2}$  of the optical amplitudes only depends on the rescaled limit-cycle amplitude,  $BJ/\kappa$ , and the mechanical frequency shift  $\mathcal{E}$ . It does not explicitly depend on the optical and mechanical detunings.

In following, we set  $\Delta_O = \Delta_M = 0$  to present the important features of the steady states. These features are not changed by finite detunings. We discuss the effects of including finite detuning at the end of this section. By

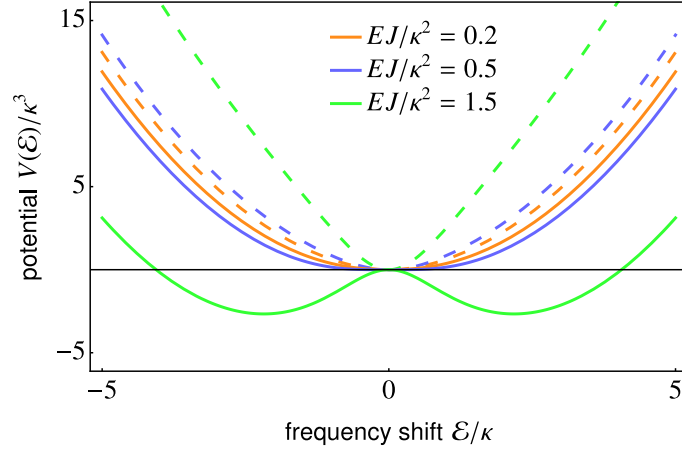


FIG. S1. The potential for the mechanical frequency shift. It has a single minimum at  $\mathcal{E} = 0$  for  $k = 2$  (dashed lines) when the higher optical frequency is driven. For  $k = 1$ , when the lower optical frequency is driven, the single minimum  $\mathcal{E} = 0$  becomes unstable with increasing  $EJ/\kappa^2$  as two minima with a finite frequency shift emerge (solid lines). (The potential is plotted for  $BJ/\kappa = 0.5$ .)

substituting the stationary values of the optical amplitudes (S8), (S9) into Eq. (S7), we obtain the stationary condition for the mechanical frequency shift

$$0 = \dot{\mathcal{E}} = -\kappa\mathcal{E} \frac{\left(\frac{\mathcal{E}}{\kappa}\right)^2 + 4 \left[ \left(\frac{JB}{\kappa}\right)^2 + \frac{1}{4} \right]^2 + 4(\delta_{2,k} - \delta_{1,k}) \left(\frac{EJ}{\kappa^2}\right)^2}{\left(\frac{\mathcal{E}}{\kappa}\right)^2 + 4 \left[ \left(\frac{JB}{\kappa}\right)^2 + \frac{1}{4} \right]^2}. \quad (\text{S10})$$

For  $k = 2$ , the mode with the higher optical frequency,  $a_2$ , is driven, only the trivial stationary solution,  $\mathcal{E} = 0$ , exists. For  $k = 1$ , the mode with the lower optical frequency,  $a_1$ , is driven, stationary solutions with a finite mechanical frequency shift

$$\mathcal{E}_{\pm} = \pm 2\kappa \sqrt{\left(\frac{EJ}{\kappa^2}\right)^2 - \left[ \left(\frac{JB}{\kappa}\right)^2 + \frac{1}{4} \right]^2} \quad (\text{S11})$$

exists, in addition to  $\mathcal{E} = 0$ , for  $4EJ/\kappa^2 > 4(BJ/\kappa)^2 + 1$ .

To gain intuition about the stability of these stationary solutions, we find the potential

$$V(\mathcal{E}) = \frac{\kappa^3}{2} \left( \left(\frac{\mathcal{E}}{\kappa}\right)^2 + 4(\delta_{2,k} - \delta_{1,k}) \left(\frac{JE}{\kappa^2}\right)^2 \ln \left( \left(\frac{\mathcal{E}}{\kappa}\right)^2 + 4 \left[ \left(\frac{JB}{\kappa}\right)^2 + \frac{1}{4} \right]^2 \right) \right), \quad (\text{S12})$$

such that  $-dV(\mathcal{E})/d\mathcal{E}$  is equal to the right hand side of Eq. (S10). The potential shows that the stationary solution  $\mathcal{E} = 0$  is always a stable steady state for  $k = 2$  when the optical mode with the higher optical frequency is driven (see Fig. S1). The stability of the steady state does not depend on the system parameters. For  $k = 1$ , when the mode with the lower optical frequency is driven, the stability of the steady state depends on the two dimensionless parameters  $EJ/\kappa^2$  and  $BJ/\kappa$ . The potential in Fig. S1 shows that the steady state  $\mathcal{E} = 0$  is the only stationary solution and it is stable in the white region of the phase diagram depicted in Fig. 2 of the main text. It becomes unstable as the two steady states with a finite mechanical frequency shift emerge in the colored region of the phase diagram in Fig. 2 of the main text. Note that the potential does not provide conclusive information about the stability of the steady states because it does not take into account the dynamics of the optical modes. Therefore, the linear stability analysis was used to confirm that the stability of the steady states is determined correctly by the potential  $V(\mathcal{E})$ .

A finite laser detuning modifies the steady states found for  $\Delta_O = 0$ . First of all, it suppresses the coherent driving, which is reflected in smaller optical amplitude of the driven mode. Furthermore, the detuning changes the potential for the mechanical frequency shift. However, the nature of its minima remains the same. There is always a unique steady state, which becomes unstable as another pair of steady states emerges, when the mode with the lower optical frequency is driven. The finite optical detuning shifts the region of bistability in the phase diagram. A new feature

is that the mechanical frequency shift  $\mathcal{E}$  is also finite in the unique steady state. The unique steady state is always stable when the mode with the higher optical frequency is driven. The finite laser detuning does not destroy the nonreciprocal property of the steady states.

A finite mechanical detuning,  $\Delta_M \neq 0$ , also modifies the mechanical frequency shift in the steady states. However, it does not change their nature. There is always a unique steady state which becomes unstable as a pair of bistable steady states emerges. This happens again only when the mode with the lower optical frequency is driven. The region of bistability is shifted in the phase diagram by the finite mechanical detuning. The mechanical frequency shift  $\mathcal{E}$  is finite also in the unique steady state due to the finite mechanical detuning.

### EQUATIONS OF MOTION FOR THE ONE-DIMENSIONAL ARRAY

Here we present the equations of motion for the one-dimensional array depicted in Fig. 1 of the main text. We consider an array composed of  $n$  sites with site  $d$  being resonantly driven. The phonon-assisted photon tunneling process is assumed to be resonant between all neighboring sites. The optical frequencies are chosen to increase with the increasing index of the site  $j$ , i.e.,  $\nu_j < \nu_{j+1}$ . The coupled equations of motion for the optical amplitudes and the mechanical phases read

$$\dot{\phi}_j = -\frac{J}{B} \text{Re} [a_j^* a_{j+1} e^{-i\phi_j}], \quad (\text{S13})$$

$$\dot{a}_j = -iE_j \delta_{j,d} - iJB e^{-i\phi_j} a_{j+1} - iJB e^{i\phi_{j-1}} a_{j-1} - \frac{\kappa}{2} a_j, \quad (\text{S14})$$

where  $\delta_{j,d}$  is the Kronecker delta. The optical modes are expressed in the frames rotating with their frequencies  $\nu_j$  and the mechanical modes are in the frames rotating with the difference of optical frequencies on the neighboring sites:  $\nu_{j+1} - \nu_j$ .